applied optics

Accuracy of retrieving optical properties from liquid tissue phantoms using a single integrating sphere

VINOIN DEVPAUL VINCELY AND KARTHIK VISHWANATH*

Department of Physics, Miami University, Oxford, Ohio 45056, USA
**Corresponding author: vishwak@miamioh.edu*

Received 22 September 2021; revised 29 November 2021; accepted 30 November 2021; posted 6 December 2021; published 3 January 2022

Using integrating spheres (ISs) in conjunction with the inverse adding–doubling algorithm (IAD) offers a well-established, rigorous protocol for determining optical absorption (μ_a) and reduced scattering (μ_s') coefficients of thin, optically homogeneous, turbid media. Here, we report the performance and use of a single IS system for experimentally retrieving optical properties in phantom media whose optical properties were well controlled. The IS system was used to measure the total reflectance and transmittance between 500 and 800 nm in liquid phantoms that were prepared to span a wide range of optical scattering and absorption coefficients. Measurements on phantoms were sequentially made using one of two broadband light sources—a halogen lamp or a supercontinuum laser. We report on the accuracy of IAD-derived optical coefficients using IS measurements made on phantoms—directly or by employing one of two previously reported correction methods. The first (sample-substitution error) correction was experimentally achieved while the second used Monte Carlo-based corrections with IAD. When experimentally calibrated reflectance and transmittance values were directly used as inputs to the IAD, mean absolute errors in recovered optical coefficients were larger than 0.4 cm^{-1} for absorption and more than 6 cm^{-1} for scattering across all phantoms and wavelengths measured. These errors reduced to 0.06–0.17 cm^{-1} and 0.7–2 cm^{-1} for μ_a and μ_s', respectively, with the use of corrections. Choice of light sources used, sample geometry (relative to optical coefficients), signal-to-noise of measurements, and the selection of correction methods are discussed.

https://doi.org/10.1364/AO.443854

1. INTRODUCTION

Non-invasive optical characterization of biological tissues using diffuse optical spectroscopy has been widely explored for its utility in diagnostic, therapeutic, and surgical applications [1–4]. Diagnostic applications include monitoring blood oxygenation or tissue metabolism, while therapeutic and surgical implementations include laser surgery and photodynamic therapy [1–3]. In applications, it is important to accurately parameterize optical properties of the media under study, which are minimally specified using wavelength-dependent absorption (μ_a) and reduced scattering (μ_s') coefficients [4,5]. Knowledge of these transport coefficients not only provides insight into tissue physiology and function but are also required for calculation of the optical energy and power delivered inside tissue media in photodynamic therapy applications [1–5].

Determining the optical properties of a sample requires use of theoretical photon-migration models, which can be either analytical or stochastic (numerical) in nature. These photon migration models operate in a forward fashion, i.e., given the optical properties of a medium and source–detector geometry needed, the photon energy distribution within and from the medium are calculated [6,7]. However, estimating optical properties from experimental measurements requires photon migration models to be iteratively used to match experimentally measured quantities—in the inverse fashion.

The radiative transport equation (RTE) is an analytical expression heuristically derived by balancing microscopic radiant energy transport in an optically turbid medium and provides a rigorous mathematical framework to model light transport in such media [6,8–10]. However, closed-form solutions to the RTE in 3D remain to be obtained, and though numerical solutions are available, they are computationally expensive [6,10]. In practice, the RTE is usually approximated using photon diffusion theory, which in turn has closed-form solutions [11]. However, diffusion theory has strict validity regimes and is known be inaccurate for specific geometries and for media where absorption is comparable to or larger than scattering [11–13]. Monte Carlo (MC) methods are used as stochastic photon migration solvers of the RTE and allow simulation of photon transport in tissue media. MC models provide a

high degree of flexibility for creating complex tissue models and/or detection geometries, but they are computationally too expensive for direct use as inverse solvers [7–10].

The adding–doubling method (AD) is a previously well-described approach and offers a numerically efficient solver of the RTE in a 1D-slab geometry [14]. Thus, it is effective for rapidly calculating the total reflectance or transmittance of thin turbid slabs of known optical properties. The inverse implementation of the AD—the inverse adding-doubling (IAD)—uses an optimization approach to match experimentally measured inputs of total reflectance and transmittance from a thin turbid slab, to extract its optical properties [6,7,11,13–15]. The main requirement to effectively use the AD/IAD solvers, is to accurately acquire the total diffuse reflectance and transmittance from media of interest.

Integrating spheres (ISs) provide the means to accurately measure total reflectance and transmittance from thin turbid media [6]. Such measurements have been obtained using single IS or double IS configurations [16–20]. Since the double IS system facilitates simultaneous measurement of reflectance and transmittance from a sample without repositioning, it is a preferred approach for measuring fresh tissue samples [14,16]. However, it at least doubles instrumentation costs and requires determination of non-trivial correction factors to correctly describe light exchange between the two spheres [14,16,21,22]. A single IS system on the other hand is readily assembled using off-the-shelf optical components at significantly lower costs and is viable for use in applications (such as routine laboratory evaluations of phantom calibration standards) where sample repositioning is easily achieved [10,15,19,23–25].

Previous reports that used single IS systems for recovery of optical properties in turbid samples have discussed the issue of light losses in measurements, which typically lead to the overestimation of μ_a [10,15,19,23–27]. While studies have explored both optimizing and improved modeling of IS configurations to minimize errors [24,27,28], they have not systematically inspected errors in interpreting experimental data obtained from phantoms with well-controlled optical properties. Further, though several experimental and theoretical methods have been proposed to improve inverse estimation of optical properties with the IS-IAD [19,22,29,30], to the best of our knowledge, a side-by-side comparison of the impact of employed corrections, across the same set of experimental data, has not been reported. Last, IS/IAD approaches have mostly been used to measure optical properties of solid samples and is not widely explored for measuring optical properties of liquid optical phantoms [29,31,32].

Here, we employ a single IS with two different illumination configurations to estimate the broadband absorption and reduced scattering coefficients of liquid phantoms. MC modeling was first used to examine the impact of the experimentally used sample, ISs, and illumination geometries. Experimental measurements were next obtained from liquid phantoms with known optical properties and analyzed using the IAD model. Analysis of the resolving power, accuracy, and errors in IAD-derived optical coefficients of liquid phantoms relative to true (expected) values are presented.

2. METHODS

A. Experimental Methods

1. Integrating Sphere for Measuring Total Reflectance and Transmittance

The experimental system used a 15.24 cm diameter IS (Labsphere RT-060-SF, Sutton, NH, USA) with five 2.54 cm diameter ports (lining the equatorial plane of the sphere's surface) and one 1.27 cm diameter port (positioned on the north pole, used as the detection port). Figure 1 schematically illustrates different configurations required for acquisition (and correction) of measurements. Figure 1(a) shows a side view of the IS system, while Fig. 1(b) illustrates a top view for positioning of the source and sample for measurements of total reflectance. As seen in Fig. 1(c), the orientation of the sample and source for transmittance is different from Fig. 1(b). The IS was equipped with a reflective baffle (coated with the same material as the interior) and served to block any specular reflection from the sample.

Illumination was provided by a free-space beam from one of two sources: (i) a halogen lamp (HL) source with an added collimator (SLS202L Thorlabs, Newton, NJ, USA) and (ii) a supercontinuum (SC) laser (SC400, NKT Photonics, Denmark) filtered through a bandpass filter (SuperK VARIA, NKT Photonics, Denmark). The HL source had a beam diameter of approximately 1.6 cm with estimated divergence of 3.6°, while the SC had a beam diameter of nearly 0.3 cm (for bandpass of 500–800 nm) and divergence lower than 0.05°. Detected light (from either source) was collected from the IS using an optical fiber (numerical aperture of 0.39; core diameter of 0.1 cm) (Thorlabs M35L01, Newton, NJ, USA) and coupled to the entrance slit of a cooled spectrometer (StellarNet SILVER-Nova, Tampa, FL, USA). The spectral range of operation of the spectrometer was 190–1100 nm, and spectral resolution was 1 nm. The detector (16-bit CCD array) was cooled to −30°C, and the ambient (dark) noise rate of the cooled detector was lower than 2.2 counts/ms (compared with the nearly 83 counts/ms for the non-cooled detector).

2. Calibration of Acquired Data

The total reflectance (R_T) and transmittance (T_T) were calculated using measurements by normalizing against intensity spectra measured from a calibration standard and correction for detector noise as shown in Eq. (1):

$$R_T(\lambda) = \frac{I_{\text{ref}}(\lambda) - I_{\text{dark}}(\lambda)}{I_{\text{std}}(\lambda) - I_{\text{dark}}(\lambda)}, \quad T_T(\lambda) = \frac{I_{\text{trans}}(\lambda) - I_{\text{dark}}(\lambda)}{I_{\text{std}}(\lambda) - I_{\text{dark}}(\lambda)}. \tag{1}$$

Here, I_{ref} and I_{trans} correspond to the wavelength-dependent reflected and transmitted intensity spectra, respectively, measured using the IS under configurations Figs. 1(b) and 1(c). I_{std} was measured as shown in Fig. 1(c) but with no sample mounted onto the sphere. Finally, I_{dark} refers to the dark noise intensity measured by the detector when the source is blocked from the sphere in orientation described in Fig. 1(b). Acquired spectra from measurements were smoothed and linearly interpolated to yield a set of 100 (linearly spaced)

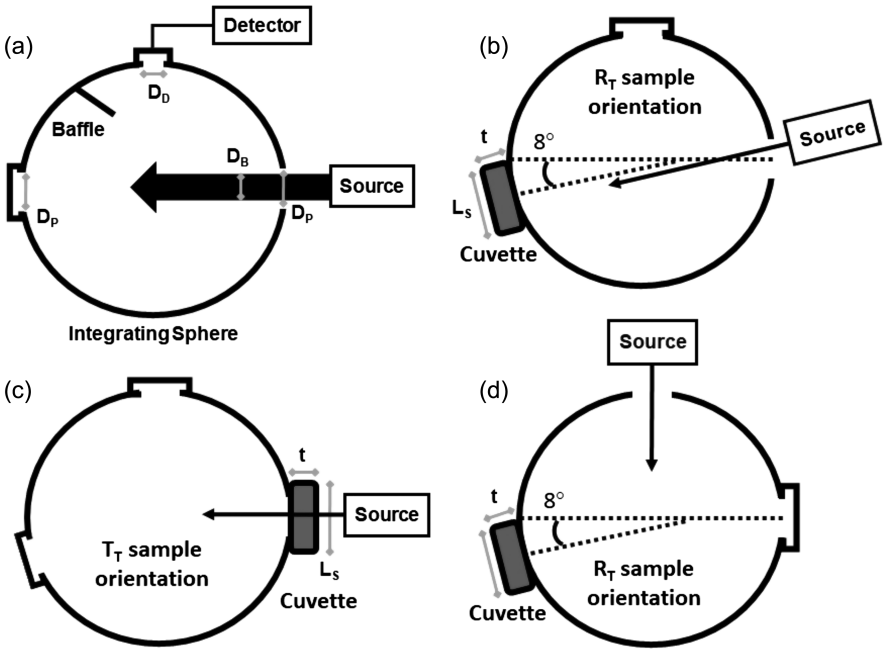

Fig. 1. (a) Side view of the single IS system schematic used (sample port diameter D_P was 2.54 cm and detector port D_D was 1.27 cm). (b)–(d) Top-view schematics for all configurations used for measurements for: (b) total reflectance, (c) total transmittance, and (d) sample substitution error corrections.

values, corresponding to wavelengths spanning 500–800 nm, for analysis.

3. *Liquid Phantoms: Preparation and Target Optical Properties*

Liquid phantoms have been widely used as gold standards for development, calibration, and validation of optical instrumentation and theoretical models in tissue optical spectroscopy [8,18,19]. They offer a simple experimental means of preparation yet are reproducible and easily characterizable. For experiments here, phantoms were prepared by mixing predetermined volumes of an absorber (typically a solution of water with a dissolved chromophore) with a scattering solution (such as a monodisperse suspension of spheres of known diameter in a solvent). For each phantom, the wavelength-dependent reduced scattering was obtained from Mie theory, while the absorption was calculated using Beer's law and transmission spectra measured from clear solutions of an absorber (Cary-100, UV-VIS, Agilent Technologies, Santa Clara, CA) [8,18].

Liquid suspensions of monodisperse 1.0 μm diameter polystyrene microspheres (07310, Polysciences, Inc., Warrington, PA) of known density provided scattering (the absorption coefficient of the sphere suspension was considered negligible), and dried bovine hemoglobin (H2625, Sigma-Aldrich, St. Louis, MO) dissolved in deionized water was used as an absorber (the scattering coefficient of this solution was assumed negligible), using previously described protocols [8,18]. Prepared phantoms were filled into a rectangular quartz cuvette that was mounted and held in contact with an IS port using a custom 3D printed mount holder such that the normal to the cuvette face was also normal to the sphere surface. The cuvette measured nearly 5 cm × 5 cm (length and height) and fully covered the port. The geometrical path length for a beam normally incident on the cuvette and transmitted through it was 0.6 cm, 0.4 cm was through cuvette walls (measuring 0.2 cm for each face), while 0.2 cm was through the liquid phantom medium.

A total of 19 liquid phantoms, each having a distinct set of optical absorption and scattering coefficients, was used in experiments here. Phantoms were prepared in two separate sets—the first phantom set (PS1) contained 10 phantoms that had low (fixed) absorption but decreasing scattering. Phantoms in PS1 were prepared by serially diluting a suspension of polystyrene microspheres such that the fraction volume of microspheres spanned 4%–30%. Hence, the absorption coefficients for all phantoms in PS1 straddled $2.38 \times 10^{-4} - 0.03\ \mathrm{cm}^{-1}$ (calculated from an absorption coefficient of pure water), while reduced scattering coefficients ranged between 2.0 and $17.6\ \mathrm{cm}^{-1}$ at 100 linearly spaced wavelengths spanning 500–800 nm (to match experimental measurements). The second phantom set (PS2) contained nine phantoms prepared by permuting three levels of scattering (20%, 30%, 40% volume of microsphere suspension) with three different concentrations of hemoglobin (16, 31, 62 μM). Expected optical properties for phantoms in PS2 spanned $0.14\ \mathrm{cm}^{-1} < \mu_a < 3.32\ \mathrm{cm}^{-1}$ and $14.5\ \mathrm{cm}^{-1} < \mu_s' < 37.1\ \mathrm{cm}^{-1}$ for the same wavelength range as PS1. The optical properties of each phantom within the two datasets are tabulated in Table 1.

B. Theoretical Models

1. *Monte Carlo Modeling of the IS System*

Previously used MC simulations [33] were modified to incorporate beam profiles (for both light sources used experimentally) and to model total reflectance and transmittance for the cuvette

Table 1. Range of Expected (Calculated) Optical Properties for Absorption and Scattering of Phantoms Used (in 1/cm)

		1	2	3	4	5	6	7	8	9	10
PS1	μ_a (cm^{-1})	$2.4 \times 10^{-4} - 2.8 \times 10^{-2}$[a]									
	μ_s' (cm^{-1})	14.9–17.7	11.9–14.1	9.5–11.3	7.6–9.1	6.1–7.2	4.9–5.8	3.9–4.6	3.1–3.7	2.5–2.9	2–2.4
PS2	μ_a (cm^{-1})	0.12–0.83	0.24–1.66	0.48–3.32	0.12–0.83	0.24–1.66	0.48–3.32	0.12–0.83	0.24–1.66	0.48–3.32	—
	μ_s' (cm^{-1})	14.5–18.6	14.5–18.6	14.5–18.6	21.8–27.8	21.8–27.8	21.8–27.8	29–37.1	29–37.1	29–37.1	—

[a]Absorption for all phantoms in PS1 was the same (see text).

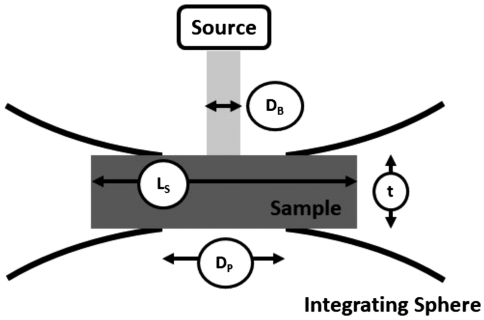

Fig. 2. Illustration of the phantom sample, the source, and IS geometry used for MC modeling. The sample is modeled as a finite square slab with side lengths (L_S) and thickness (t) mounted on the port of an IS with port diameter (D_P). The illumination beam is assumed to be collimated and of diameter (D_B) with uniform intensity. MC simulations computed the total reflected and transmitted flux collected by the sphere port for any specified sample optical properties.

(sample) geometry used [34]. Parameters of experimental interest modeled by MC simulations are illustrated in Fig. 2 and include the diameter D_B of the source beam, the lateral length (L_s) of the sample cuvette, the integrating port diameter D_p, and the thickness of the sample (t). MC simulations were used to examine changes in total collected reflectance and transmittance (a) for varying the ratio of the source beam size to the IS port size (D_B/D_P), and (b) varying sample dimensions with port size (L_S/D_P).

In MC simulations, photons were launched as moving along $+z$ at the $z = 0$ plane from a uniform beam intensity profile with diameter D_B, into the medium. The sample thickness (t) and dimensions (L_S) for all simulations were set to 0.2 cm and 5.08 cm, respectively to match experimental conditions. Finally, a circular collection area with radius 2.54 cm was defined to emulate the sample port of the IS. All photons moving along the $-z$ direction at the illuminated surface and escaping within the collection area were scored to compute the total diffuse reflectance. All photons exiting the sample at $z = d$ (moving in the $+z$ direction) within the collection area were used to calculate the total transmittance. The MC model also calculated light scattered out of the sample volume (in the $\pm x$ and $\pm y$ directions) at the medium boundaries. Thus, in each MC run for a given sample, the escaping hemispherical flux (across the six sample surfaces) was stored.

2. *Inverse Adding-Doubling for Extraction of Optical Properties*

Optical properties from a sample with given total reflectance and total transmittance (obtained from either experimental measurements or MC simulations) were extracted using the IAD model [13,35,36]. Besides measured reflectance and transmittance, the IAD also required other input parameters for estimating optical properties from inputs. These included the thickness of the sample, the sample anisotropy, and the refractive indices of the sample and the ambient media (above and below the sample). Sample thickness was set to 0.2 cm, refractive index of the medium was 1.33, and the refractive index of the ambient medium was set to 1.55 to emulate experimental conditions. Finally, the sample anisotropy was set as $g = 0.9$ (which was obtained from an average Mie theory value between 500 and 800 nm for the polystyrene spheres) [11,14,15,19,22].

C. Corrections to Measured Reflectance and Transmittance

Studies have previously reported discrepancies between IAD computed optical properties as resulting from incorrect measurements of total reflectance and transmittance [10,19,24,27,28,30,37]. IS measurements are known to exhibit a loss in the total fluence collected, which are exacerbated when samples have lower reflectance than the standards used for calibration [10,22,25,26,30]. Experimentally, the R_T values can be corrected for such losses using the substitution method, where sample intensities are normalized by reflectance measured using the sample [15,22,25] as illustrated in Fig. 1(d). Thus, for substitution correction the total reflectance was computed using the diffuse illumination (I_{diff}) of sample as

$$R_T(\lambda) = \frac{I_{\text{ref}}(\lambda) - I_{\text{dark}}(\lambda)}{I_{\text{diff}}(\lambda) - I_{\text{dark}}(\lambda)}. \quad (2)$$

Experimentally corrected total reflectance obtained using Eq. (2) along with the total transmittance from each sample were then used as inputs to the IAD for retrieving absorption and reduced scattering values for all measured wavelengths.

Independently, systemic losses in IS measurements can also be corrected by modeling total power collected by the IS as a function of the sphere's geometric and reflection parameters [17]. This approach, coupled with a hybrid MC approach for correcting fluence losses in IS measurements from finite sizes of IS ports, is available within the publicly available IAD software suite [35,36]. As a second correction scheme, power corrections for IS with inbuilt MC-based calibrations in the IAD were switched on for prediction of optical properties. Incorporating the IAD-MC correction slowed inverse calculations by nearly 20–30 times, relative to IAD calculations without the power losses or MC simulations toggled on. We refer to this second correction approach as the IAD-MC approach. Details of

switches used in IAD for the IAD-MC corrections are provided in Supplement 1.

3. RESULTS

A. Internal Consistency and Sensitivity of the IAD

Internal consistency and sensitivity of IAD-derived optical coefficients was first assessed by directly using the AD model to generate inputs that were provided to IAD. For these analyses, the AD was used to compute total reflectance and transmittance in 600 media, each with different sets of optical properties permuted from 30 values of μ_a ($0.04-4\ \mathrm{cm}^{-1}$) and 20 values of μ_s' ($3\ \mathrm{cm}^{-1}-30\ \mathrm{cm}^{-1}$). When analyzed with IAD, results showed that absorption and reduced scattering coefficients retrieved were accurate to within $5 \times 10^{-4}\ \mathrm{cm}^{-1}$ and $0.1\ \mathrm{cm}^{-1}$, respectively. Additionally, we observed that the accuracy of retrieving the absorption coefficient was highly sensitive to noise. The input reflectance and transmittance values—a perturbation of 1% in input values—resulted in differences of nearly $0.01\ \mathrm{cm}^{-1}$ in absorption coefficients, while a 10% perturbation linearly increased this difference to $0.1\ \mathrm{cm}^{-1}$. Similarly, a 1% perturbation of input values resulted in a change of $0.2\ \mathrm{cm}^{-1}$ in recovered reduced scattering coefficient, while a 10% perturbation resulted in differences of nearly $2\ \mathrm{cm}^{-1}$.

B. Impact of Source and Sample Geometry Using MC Simulations

MC models (described in Section 2.B.1) were used to calculate total reflectance and transmittance values from sample and illumination geometries used experimentally. A total of 300 simulations was performed for illumination configurations of the HL and the SC source—where MC models changed input beam diameters for the two sources and was set to 1.6 cm for the HL source and to 0.3 cm for the SC source. Both sources were modeled as having uniform beam intensity profiles when incident on the sample. Optical properties used in these simulations were obtained by permuting 15 different absorption coefficients ($0.04-4\ \mathrm{cm}^{-1}$) with 20 reduced scattering ($3-30\ \mathrm{cm}^{-1}$) coefficients (both coefficients were logarithmically evenly spaced). The simulated total reflectance and transmittance from MC models were used as inputs into IAD to retrieve optical properties.

Figure 3 depicts results of these analyses and as shows the absolute and percent differences between IAD-derived optical properties versus the true values (used to generate MC simulations). Figures 3(a) and 3(c) show the absolute and percent errors in retrieved absorption, while Figs. 3(b) and 3(d) show the absolute and percent errors in recovered scattering coefficients. In these figures, data are shown from media that had fixed scattering (for two different scattering levels) but with varying absorption [Figs. 3(a) and 3(c)], or for media that had fixed

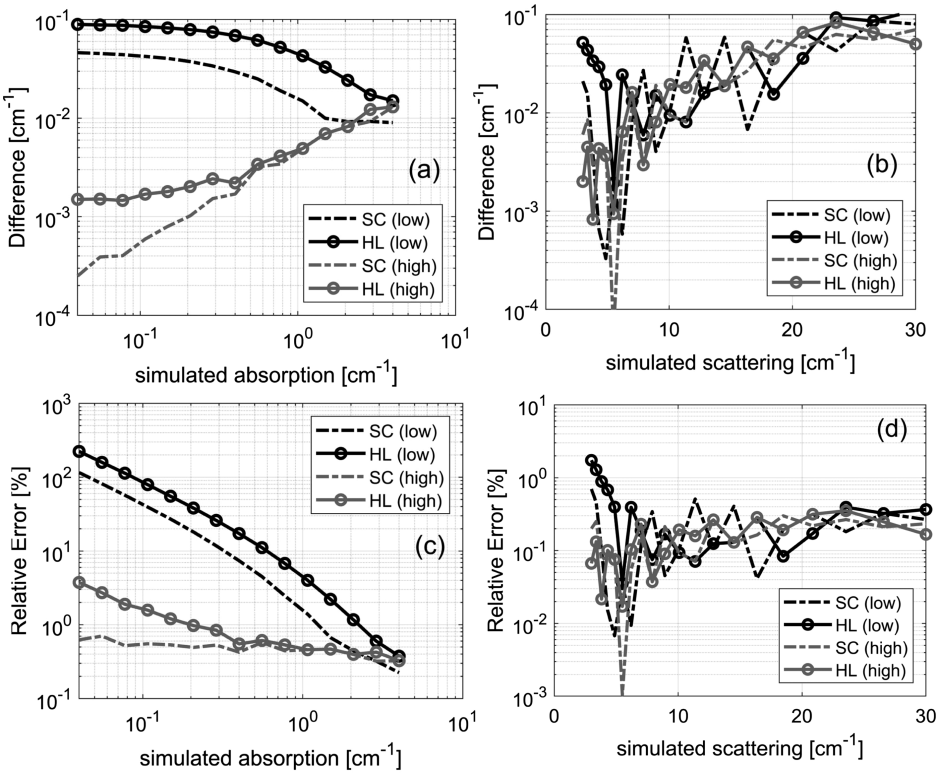

Fig. 3. (a), (b) Absolute differences and (c), (d) percent errors between IAD-derived optical properties and the input values used in MC simulations. (a), (c) Absolute differences and percent errors between IAD-derived and true values as a function of the absorption, respectively. (b), (d) Absolute and percent errors in scattering, respectively. Dashed lines correspond to simulations done with illumination beam diameter set to 0.3 cm, while circles correspond to simulations with 1.6 cm beam diameter. The gray curves in (a) and (c) represent simulation results with a constant scattering value of $30\ \mathrm{cm}^{-1}$, while those in (b) and (d) represent simulation results with a constant absorption value of $4\ \mathrm{cm}^{-1}$. Finally, the black curves in (a) and (c) represent simulation results with a constant scattering value of $3\ \mathrm{cm}^{-1}$, while those in (b) and (d) represent simulation results with a constant absorption value of $0.04\ \mathrm{cm}^{-1}$.

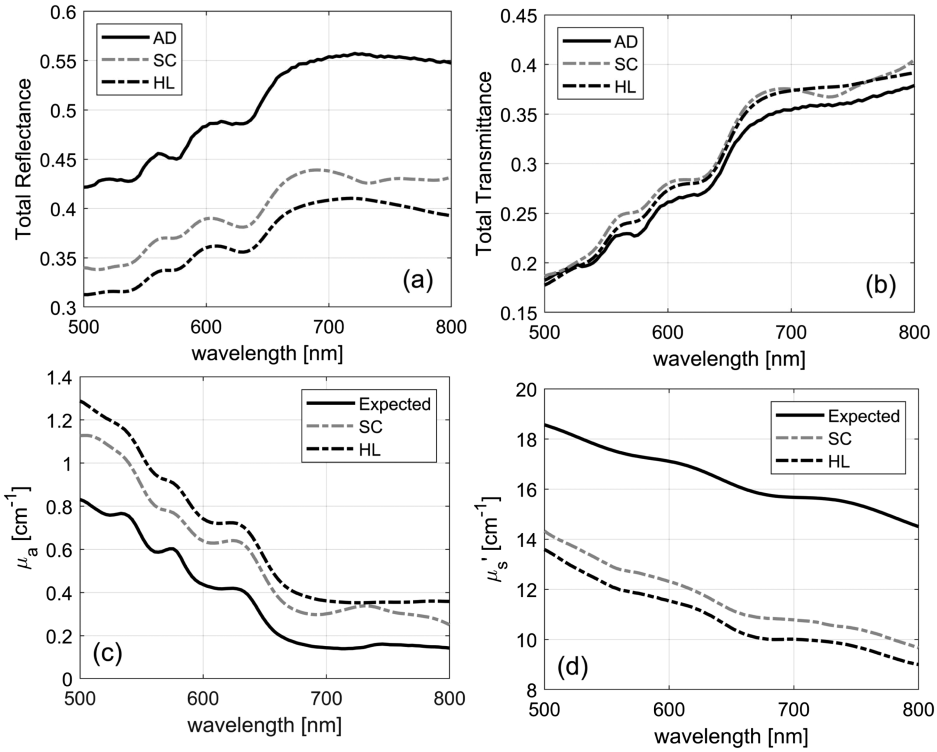

Fig. 4. Representative measurements of reflectance and transmittance without incorporating experimental corrections. (a), (b) Measurements (reflectance and transmittance, respectively) for phantom-1 (in PS2) for both sources (HL: black dotted line; SC: light gray dotted line) as well as forward calculations using the AD given the expected optical coefficients of the phantom (solid black line). (c), (d) Derived optical absorption and reduced scattering coefficients using the measurements shown in (a) and (b) for each illumination source (HL: black dotted line; SC: light gray dotted line) together with the expected optical coefficients (solid black line) for the phantoms used as inputs to the AD.

absorption (for two different absorption levels) and varying scattering [Fig. 3(b) and 3(d)]. Absolute and percent errors in recovered absorption coefficients are shown in Figs. 3(a) and 3(c) using gray lines and symbols for media with highly scattering media ($\mu_s' = 30\ \mathrm{cm}^{-1}$), while black lines and symbols represent results for the low scattering media ($\mu_s' = 3\ \mathrm{cm}^{-1}$). Similarly, errors for retrieved scattering in gray and black represent media with high ($\mu_a = 4\ \mathrm{cm}^{-1}$) and low absorption ($\mu_a = 0.04\ \mathrm{cm}^{-1}$), respectively, in Figs. 3(b) and 3(d) and are plotted on a logarithmic scale. All figures show data modeled from both sources (dashed lines: SC; circles: HL).

These analyses indicate that errors in recovered μ_a were large (>100%) for simulations with low scattering ($\approx 0.4\ \mathrm{cm}^{-1}$) and low absorption ($<0.1\ \mathrm{cm}^{-1}$) for either source configuration. However, errors in absorption were low (<10%) as sample absorption increased ($>1\ \mathrm{cm}^{-1}$) or if the sample scattering increased ($\sim 30\ \mathrm{cm}^{-1}$). Interestingly, errors in recovered scattering were lower than 1%.

C. Direct Comparison of Experimental Measurements with AD and IAD

IS measurements were made for each phantom in both phantom sets—PS1 and PS2—using both HL and SC as illumination sources, sequentially. Figures 4(a) and 4(b) show measured total reflectance and transmittance from the IS system along with predicted values (derived from the AD model with given inputs of expected optical properties of the phantom). Data shown are from the first phantom in PS2 (hemoglobin concentration of 16 μM with 20% volume of PS spheres). As seen in Figs. 4(a) and 4(b), there is better agreement between the measured and predicted transmittance values, but there is a clear mismatch between predicted reflectance (from AD) and measured values, for both light sources.

These measurements were translated into optical properties using IAD and compared to the expected values of the absorption and scattering coefficients (for the specific phantom) and are shown in Figs. 4(c) and 4(d), respectively. As a result of the losses in total reflectance, the derived optical properties were significantly different from their expected values. These observations were consistent across all phantoms measured, with predicted absorption coefficients being higher than expected (true) values and were attributable to a lower-than-expected measured reflectance. The IAD-derived reduced scattering was also lower than those expected values (from Mie theory) as illustrated in Fig. 4(d). Last, errors in both coefficients were higher for the HL source, relative to those obtained from the SC source.

D. Estimation of Optical Properties Post Corrections

Experimental measurements were analyzed by applying each correction method (described in Section 2.B) in all phantoms measured for both illumination configurations. The sample substitution correction was experimentally achieved, while the second method enabled IAD-MC for analyses. Figures 5(a) and

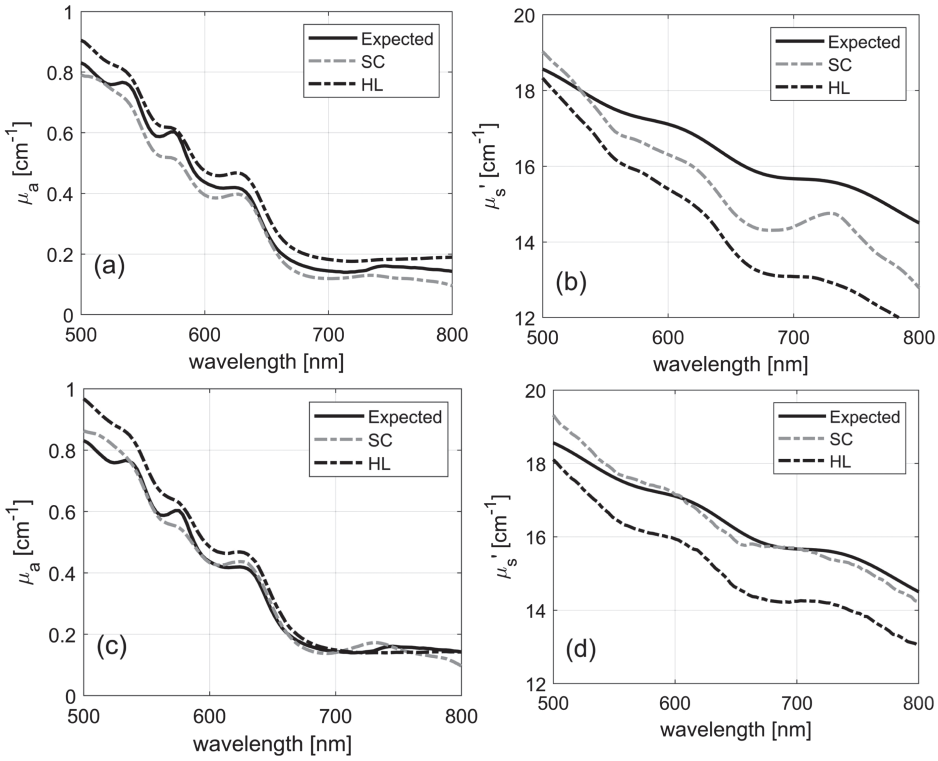

Fig. 5. IAD-derived optical properties using various experimental configurations. (a), (b) IAD predictions of the optical absorption and reduced scattering coefficients, respectively, for phantom-1 (PS2) under the substitution correction method for both sources (HL: black dotted line; SC: light gray dotted line) as well as the expected optical coefficients of the phantom (solid black line). (c), (d) Derived optical absorption and reduced scattering coefficients with incorporating the IAD-MC correction method for each illumination source (HL: black dotted line; SC: light gray dotted line) together with the expected optical coefficients (solid black line) of phantom-1 (PS2).

5(b) show derived absorption and reduced scattering coefficients for the same phantom (first phantom in PS2 set) shown in Fig. 4, but after applying the sample-substitution correction. Correspondingly, Figs. 5(c) and 5(d) show the derived absorption and reduced scattering coefficients, with the IAD-MC corrections. Errors in the derived optical coefficients decreased significantly (relative to those shown in Fig. 4), with both correction methods, for both sources.

To consolidate and analyze errors in retrieved optical coefficients between 500 and 800 nm in all measured phantoms with each light source, we consider the distribution of the errors in IAD-derived coefficients [computed as the difference between estimated (retrieved) optical coefficients and the expected (true) values], as a function of the true values of the optical coefficients. However, given the large range of values spanned in the phantoms together with the spectral dependence of optical coefficients, the distribution of optical coefficients was not uniform across the range of values spanned. Thus, to facilitate a uniform error analysis, we binned optical absorption (scattering) coefficients with variable bin widths (ranges) such that bin widths chosen ensured uniform distribution of optical coefficients. This procedure was applied separately for all phantoms in PS1 (Fig. 6) and then repeated again for all phantoms in PS2 (Fig. 7) since phantom sets PS1 and PS2 had distinctly differing absorption profiles.

Figure 6 shows distribution differences in retrieved and expected values of μ_a [Fig. 6(a): HL source; Fig. 6(c) SC source] and μ_s' [Fig. 6(b): HL source; Fig. 6(d) SC source] across the 10 phantoms in PS1. Vertical bars represent mean values of differences for all optical coefficients in the group, while the error bars represent standard deviations. Each figure shows data for analysis without any corrections (light gray bars), with the sample substitution correction (dark gray bars) and the IAD-MC corrections (black bars). Labels on the horizontal axis identify bin center and widths. Data in Fig. 6 reiterate the patterns observed in Fig. 5—that when IS measurements were analyzed without corrections (light gray bars), they produced optical coefficients that large differences from their expected values. Both the sample substitution (dark gray bars) and IAD-MC (black bars) corrections significantly improved these estimates, for both optical coefficients and measurements using either source.

Figure 7 shows distributions of differences in retrieved and expected values of optical absorption [Fig. 7(a): HL source; Fig. 7(c) SC source] and for reduced scattering coefficients [Fig. 7(b): HL source; Fig. 7(d) SC source] using data from nine phantoms in PS2. As in Fig. 6, bars represent mean values of differences of optical coefficients for each bin, while the error bars show standard deviations. It is worth noting that the expected absorption and scattering properties for the phantoms in Fig. 7 (PS2) are distinctly different from those in Fig. 6 (PS1).

Table 2 summarizes the mean precent errors between the extracted optical coefficients using measurements using both light sources for all three inverse methods (no correction,

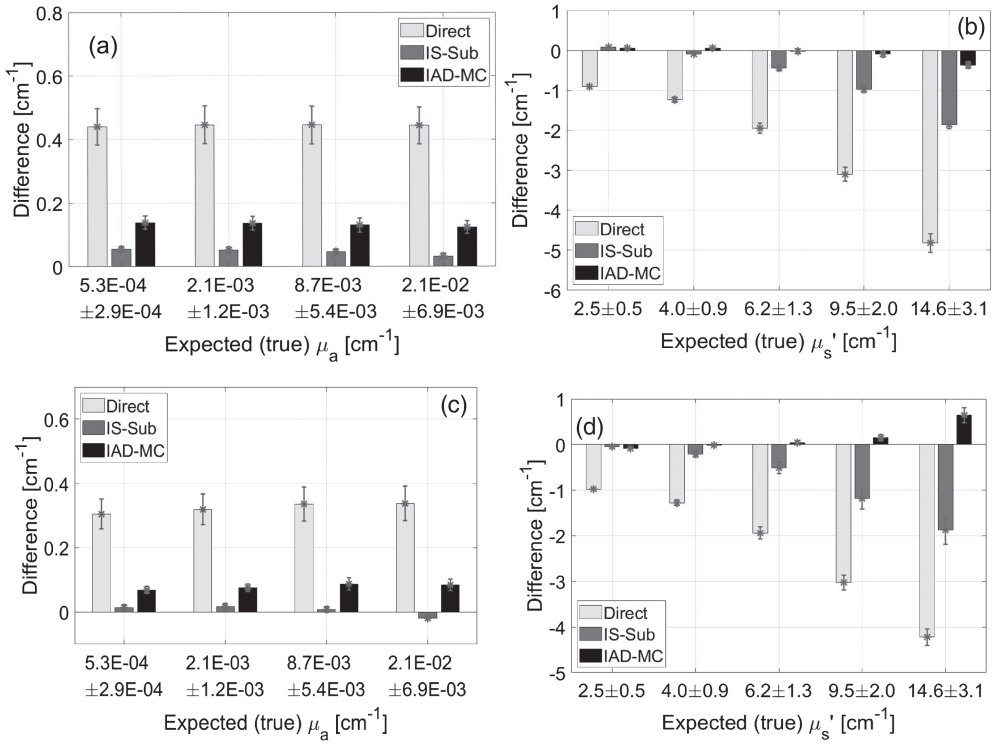

Fig. 6. Distribution of the differences between the derived values (light gray: no correction; dark gray: with substitution error correction; black: MC based correction) and the expected (true) values of absorption coefficients for (a) HL source and (c) SC source across the range of absorption coefficients spanned by 10 phantoms in phantom set PS1. (b), (d) Differences between derived and true values for the reduced scattering coefficients using measurements, for the same set of 10 phantoms in PS1 using measurements from the HL and SC source, respectively. The range of values spanned used for binning are as noted on the x axis and were determined so that the frequency count for these ranges resulted in uniform numbers of samples per bin (see text).

Table 2. Summary of Mean Percent Errors (and Standard Deviations in Parentheses) in Derived Optical Coefficients from IS Measurements via IAD Inverse Calculations[a]

	HL Source		SC Source	
Method	μ_a	μ_s'	μ_a	μ_s'
No correction	45.3 (43.8)	−32.4 (3.6)	43.4 (41.0)	−30.1 (5.3)
Substitution	−10.4 (19.5)	−7.7 (7.5)	−18.2 (15.4)	−5.3 (6.4)
IAD-MC	−18.5 (22.4)	−1.9 (3.7)	−9.2 (17.1)	1.1 (3.1)
Substitution + IAD-MC	−62.8 (27.2)	26.8 (8.5)	−60.7 (26.4)	37.6 (4.8)

[a]As noted in the text, the errors in absorption are only shown for phantoms in PS2, but the errors in scattering are for all phantoms in PS1 and PS2.

substitution error, and IAD-MC). As seen in Figs. 6(a) and 6(c), for media with low absorption values (lower than about 0.05 cm^{-1}), the retrieved absorption coefficients exceeded the true values (frequently by over two orders of magnitude), and thus, the data in Table 2 for percent errors in absorption included only data from phantoms in data set PS2 (Fig. 7), since all phantoms in PS2 included hemoglobin as an absorber. However, for errors in reduced scattering, the data in Table 2 were compiled using all 19 phantoms in PS1 and PS2.

Table 2 also shows a fourth method that incorporated both substitution and IAD-MC corrections, and as seen, the overall errors in both retrieved absorption and scattering become as poor as having no corrections. Representative data of this behavior with both corrections used together is shown in Supplement 1, Fig S1.

4. DISCUSSION

A single IS-based system was used to measure the total reflectance and transmittance in liquid phantoms across 500–800 nm using one of two light sources (HL and SC). IS measurements were calibrated to provide inputs to the IAD algorithm, which translated them into optical coefficients of absorption and reduced scattering. Optical properties from IAD were obtained by directly using (calibrated) IS measurements, or after correcting measurements by a correction method—an experimental (sample substitution) correction, or a numerically applied IAD-MC correction.

Optical properties that were closest to expected values in phantoms were obtained using the SC source with IAD-MC correction approach with mean absolute (percent) errors in retrieved absorption and scattering of 0.018 cm^{-1} (9.2%) and 0.36 cm^{-1} (1.1%), respectively. Upon correction with sample substitution, the HL source provided estimates that were nearly as good as the SC for scattering and had lower average absolute (relative) errors in absorption errors (seen in Table 2). Either correction method significantly improved, for either light source, the derived absorption and scattering coefficients from

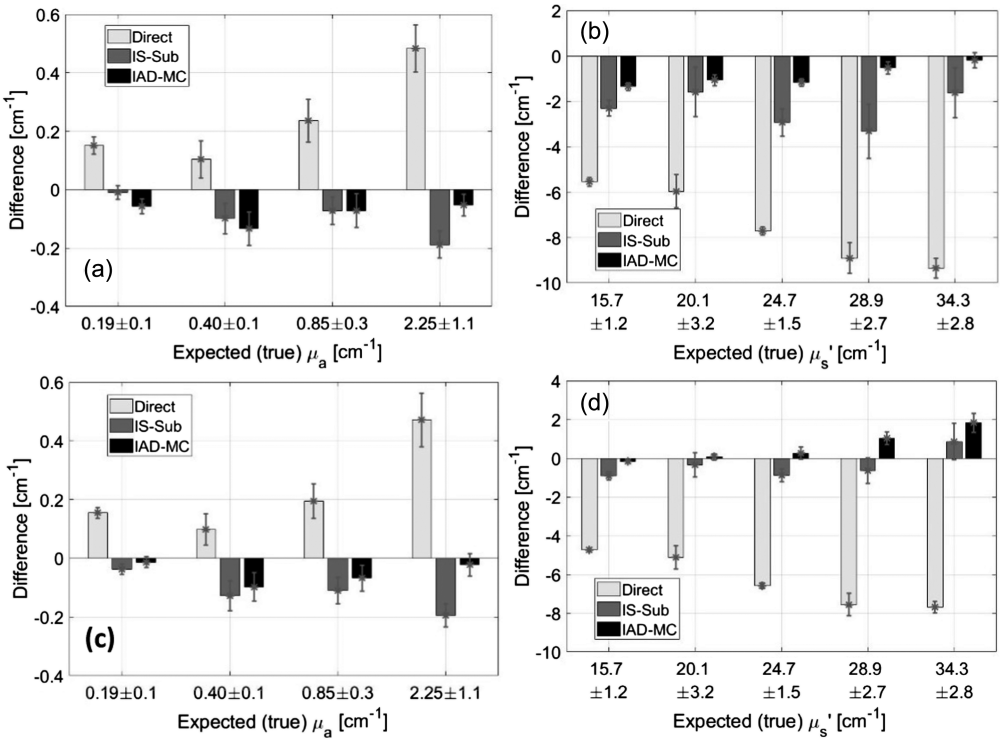

Fig. 7. Distribution of the differences between the derived values (light gray: no correction; dark gray: with substitution error correction; black: MC based correction) and the expected (true) values of absorption coefficients for (a) HL source and (c) SC source across the range of absorption coefficients spanned by nine phantoms in phantom set PS2. (b), (d) Differences between derived and true values for the reduced scattering coefficients using measurements, for the same set of nine phantoms in PS2 using measurements from the HL and SC sources, respectively.

phantoms, relative to no corrections. Applying both correction methods together worsened errors in derived coefficients.

Given the markedly different source profiles between the SC and HL sources used, it is interesting to observe that when ISs measured reflectance and transmittance used directly in the IAD, they both showed errors of more than 30% in derived optical coefficients for all phantoms in PS2. Consequently, these errors cannot then be directly attributable to the beam profiles and geometries of the sources. Effects of optical polarization also would be expected to be insignificant, as both the reflected and transmitted light traverses a highly scattering medium, and it has been reported that light exiting the IS becomes independent of the polarization of the incident light [38]. The fact that either correction method used reduces errors indicates that correction of power loss in the total fluence collected by the IS mitigated the issue of measuring lower reflectance [Fig. 4(a)] [25,26]. Since both these corrections compensate for a reduced reflectance, using them in conjunction results in an over correction and leads to worsened performance (seen in Table 2 and Supplement 1, Fig. S1).

Accuracy of retrieving the absorption coefficient was dependent on the scattering of the sample—with lower errors found in samples with high scattering. MC simulations indicate that for our sample and IS geometry used, the probability of photons escaping the edges of the cuvette wall (and thus not making it into the IS for detection) increased with reduced scattering [34]. This could explain why phantoms with higher scattering showed better reconstructions for the optical coefficients.

The sensitivity to changes measured in reflectance for samples with low absorption are ultimately limited by detector sensitivity and noise. In our system, the spectrometer dark count rate was nearly 1.5 counts/ms and translated to a lower limit of 0.01 cm^{-1} in measurable absorption. Thus, reconstructions of absorption values of phantoms in PS1 were poor overall. In samples that had low scattering together with low absorption, even the transmittance measurements can quickly saturate detectors and need to be carefully monitored.

5. CONCLUSION AND FUTURE WORK

In this study, a single IS coupled with the IAD algorithm was used for extraction of optical properties from experimental measurements. Thin, turbid homogeneous liquid phantoms that spanned optical properties relevant to biological tissues were used to characterize the common sources of experimental errors that yield inaccuracies in retrieved optical properties. We have limited our imaging systems to span the spectral range commonly spanned by diffuse optical spectroscopy methods.

We found that it was possible to use a weakly collimated and diverging HL source with a cooled (portable) spectrometer to extract wavelength-dependent optical absorption and reduced scattering of optically turbid liquid samples with errors of under 10%. However, IS measurements of total reflectance and transmittance need to be corrected to account for a systematic loss in the fluence detected in the IS. The two correction approaches described here serve equally well for improving extraction of optical properties from measurements.

Overall, it was possible to extract the reduced scattering robustly, while accuracy of the extracted absorption coefficient was dependent on the scattering coefficients of the medium. These limitations reside in the signal–noise present in the measurements and can be improved by using detectors with low dark noise. Beam collimation and divergence only marginally impacted retrieval of optical coefficients. We also limited our focus in using the IS/IAD approach for estimations of absorption and reduced scattering coefficients only.

One aspect that remains to be studied in relation to the issue resolving the optical coefficients of low absorbing and scattering media is whether measurements of collimated transmittance could help alleviate it. As has been previously noted, measurements of collimated transmittance are not trivial [14,15,26]. Additionally, the impact of (known) variations in the anisotropy of phantoms could also be modeled by the IAD. These topics will be investigated in the future.

Funding. Miami University.

Disclosures. The authors declare no conflicts of interest.

Data Availability. Data underlying the results presented in this paper are not publicly available at this time but may be obtained from the authors upon reasonable request.

Supplemental document. See Supplement 1 for supporting content.

REFERENCES

1. J. C. Li and K. Y. Pu, "Development of organic semiconducting materials for deep-tissue optical imaging, phototherapy and photoactivation," Chem. Soc. Rev. **48**, 38–71 (2019).
2. Y. Hoshi and Y. Yamada, "Overview of diffuse optical tomography and its clinical applications," J. Biomed. Opt. **21**, 091312 (2016).
3. G. Balasundaram, C. Krafft, R. C. Zhang, K. Dev, R. Z. Bi, M. Moothanchery, J. Popp, and M. Olivo, "Biophotonic technologies for assessment of breast tumor surgical margins-a review," J. Biophoton. **14**, e202000280 (2021).
4. M. Ferrari and V. Quaresima, "A brief review on the history of human functional near-infrared spectroscopy (fNIRS) development and fields of application," Neuroimage **63**, 921–935 (2012).
5. R. H. Wilson, K. Vishwanath, and M. A. Mycek, "Optical methods for quantitative and label-free sensing in living human tissues: principles, techniques, and applications," Adv. Phys. X **1**, 523–543 (2016).
6. S. R. Arridge, "Optical tomography in medical imaging," Inverse Probl. **15**, R41–R93 (1999).
7. D. T. Delpy, M. Cope, P. Vanderzee, S. Arridge, S. Wray, and J. Wyatt, "Estimation of optical pathlength through tissue from direct time of flight measurement," Phys. Med. Biol. **33**, 1433–1442 (1988).
8. J. E. Bender, K. Vishwanath, L. K. Moore, J. Q. Brown, V. Chang, G. M. Palmer, and N. Ramanujam, "A robust-Monte Carlo model for the extraction of biological absorption and scattering in vivo," IEEE Trans. Biomed. Eng. **56**, 960–968 (2009).
9. J. Q. Brown, K. Vishwanath, G. M. Palmer, and N. Ramanujam, "Advances in quantitative UV-visible spectroscopy for clinical and pre-clinical application in cancer," Curr. Opin. Biotechnol. **20**, 119–131 (2009).
10. F. Foschum, F. Bergmann, and A. Kienle, "Precise determination of the optical properties of turbid media using an optimized integrating sphere and advanced Monte Carlo simulations," Appl. Opt. **59**, 3203–3215 (2020).
11. A. N. Bashkatov, E. A. Genina, V. I. Kochubey, and V. V. Tuchin, "Optical properties of human skin, subcutaneous and mucous tissues in the wavelength range from 400 to 2000 nm," J. Phys. D **38**, 2543–2555 (2005).
12. A. Ishimaru, "Diffusion of light in turbid material," Appl. Opt. **28**, 2210–2215 (1989).
13. S. A. Prahl, M. J. C. Vangemert, and A. J. Welch, "Determining the optical-properties of turbid media by using the adding-doubling method," Appl. Opt. **32**, 559–568 (1993).
14. J. F. Beek, P. Blokland, P. Posthumus, M. Aalders, J. W. Pickering, H. Sterenborg, and M. J. C. vanGemert, "In vitro double-integrating-sphere optical properties of tissues between 630 and 1064 nm," Phys. Med. Biol. **42**, 2255–2261 (1997).
15. W. Saeys, M. A. Velazco-Roa, S. N. Thennadil, H. Ramon, and B. M. Nicolai, "Optical properties of apple skin and flesh in the wavelength range from 350 to 2200 nm," Appl. Opt. **47**, 908–919 (2008).
16. M. Hammer, A. Roggan, D. Schweitzer, and G. Muller, "Optical-properties of ocular fundus tissues - an in-vitro study using the double-integrating-sphere technique and inverse Monte-Carlo simulation," Phys. Med. Biol. **40**, 963–978 (1995).
17. J. W. Pickering, S. A. Prahl, N. Vanwieringen, J. F. Beek, H. Sterenborg, and M. J. C. Vangemert, "Double-integrating-sphere system for measuring the optical-properties of tissue," Appl. Opt. **32**, 399–410 (1993).
18. A. Kienle, M. S. Patterson, N. Dognitz, R. Bays, G. Wagnieres, and H. van den Bergh, "Noninvasive determination of the optical properties of two-layered turbid media," Appl. Opt. **37**, 779–791 (1998).
19. D. Hu, R. F. Lu, Y. P. Huang, Y. B. Ying, and X. P. Fu, "Effects of optical variables in a single integrating sphere system on estimation of scattering properties of turbid media," Biosyst. Eng. **194**, 82–98 (2020).
20. T. J. Farrell, M. S. Patterson, and B. Wilson, "A diffusion-theory model of spatially resolved, steady-state diffuse reflectance for the noninvasive determination of tissue optical-properties *in vivo*," Med. Phys. **19**, 879–888 (1992).
21. D. Zhu, W. Lu, S. Q. Zeng, and Q. M. Luo, "Effect of light losses of sample between two integrating spheres on optical properties estimation," J. Biomed. Opt. **12**, 064004 (2007).
22. G. Vriesde, J. F. Beek, G. W. Lucassen, and M. J. C. van Gemert, "The effect of light losses in double integrating spheres on optical properties estimation," IEEE J. Sel. Top. Quantum Electron. **5**, 944–947 (1999).
23. L. Vidovic and B. Majaron, "Elimination of single-beam substitution error in diffuse reflectance measurements using an integrating sphere," J. Biomed. Opt. **19**, 027006 (2014).
24. E. Terán, E. R. Méndez, R. Quispe-Siccha, A. Peréz-Pacheco, and F. L. S. Cuppo, "Application of single integrating sphere system to obtain the optical properties of turbid media," OSA Contin. **2**, 1791–1806 (2019).
25. P. Nostell, A. Roos, and D. Ronnow, "Single-beam integrating sphere spectrophotometer for reflectance and transmittance measurements versus angle of incidence in the solar wavelength range on diffuse and specular samples," Rev. Sci. Instrum. **70**, 2481–2494 (1999).
26. I. V. Yaroslavsky, A. N. Yaroslavsky, T. Goldbach, and H. J. Schwarzmaier, "Inverse hybrid technique for determining the optical properties of turbid media from integrating-sphere measurements," Appl. Opt. **35**, 6797–6809 (1996).
27. R. F. Lu, R. Van Beers, W. Saeys, C. Y. Li, and H. Y. Cen, "Measurement of optical properties of fruits and vegetables: a review," Postharvest Biol. Technol. **159**, 111003 (2020).
28. B. Liu, Y. Yuan, Z. Y. Yu, X. Huang, and H. P. Tan, "Numerical investigation of measurement error of the integrating sphere based on the Monte-Carlo method," Infrared Phys. Technol. **79**, 121–127 (2016).
29. J. Gunther, H. H. Lu, and S. Andersson-Engels, "Combination of diffuse reflectance and transmittance spectroscopy to obtain optical properties of liquid phantoms," Opt. Eng. **59**, 024109 (2020).
30. H. L. Gorton, C. R. Brodersen, W. E. Williams, and T. C. Vogelmann, "Measurement of the optical properties of leaves under diffuse light," Photochem. Photobiol. **86**, 1076–1083 (2010).
31. L. Spinelli, M. Botwicz, N. Zolek, *et al.*, "Determination of reference values for optical properties of liquid phantoms based on Intralipid and India ink," Biomed. Opt. Express **5**, 2037–2053 (2014).
32. L. Cortese, G. Lo Presti, M. Pagliazzi, D. Contini, A. Dalla Mora, A. Pifferi, S. K. V. Sekar, L. Spinelli, P. Taroni, M. Zanoletti, U. M. Weigel, S. de Fraguier, N. D. An, B. Rosinski, and T. Durduran, "Liquid phantoms for near-infrared and diffuse correlation spectroscopies with tunable optical and dynamic properties," Biomed. Opt. Express **9**, 2068–2080 (2018).

33. K. Vishwanath and M. A. Mycek, "Time-resolved photon migration in bi-layered tissue models," Opt. Express **13**, 7466–7482 (2005).
34. V. D. Vincely and K. Vishwanath, "Lateral light losses in integrating sphere measurements: comparison of Monte-Carlo with inverse adding-doubling algorithm," Proc. SPIE **11231**, 112310G (2020).
35. S. A. Prahl, "Inverse-adding doubling algorithm," 2011, https://omlc.org/software/iad/.
36. S. Prahl, "Everything I think you should know about inverse adding-doubling," 2011, https://omlc.org/software/iad/manual.pdf.
37. X. W. Zhong, S. X. Tan, X. Wen, and D. Zhu, "Effect of light beam on measurements of reflectance and transmittance of turbid media with integrating sphere: Monte Carlo simulation," Front. Optoelectron. **8**, 203–211 (2015).
38. S. C. McClain, C. L. Bartlett, J. L. Pezzaniti, and R. A. Chipman, "Depolarization measurements of an integrating sphere," Appl. Opt. **34**, 152–154 (1995).